THE JOURNAL OF PHYSICAL CHEMISTRY B

Article

pubs.acs.org/JPCB

Cation Dynamics in the Pyridinium Based Ionic Liquid 1-*N*-Butylpyridinium Bis((trifluoromethyl)sulfonyl) As Seen by Quasielastic Neutron Scattering

Jan P. Embs,*[,†] Tatsiana Burankova,[†,‡] Elena Reichert,[‡] and Rolf Hempelmann[‡]

[†]Laboratory for Neutron Scattering, Paul Scherrer Institut, Villigen-PSI, Switzerland

[‡]Department of Physical Chemistry, Saarland University, Saarbrücken, Germany

ABSTRACT: Quasielastic neutron scattering (QENS) has been used to study the cation dynamics in the pyridinium based ionic liquid (IL) 1-*N*-butylpyridinium bis-((trifluoromethyl)sulfonyl)imide (BuPy-Tf_2N). This IL allows for a detailed investigation of the dynamics of the cations only, due to the huge incoherent scattering cross section of the cation ($\sigma_{inc}^{cation} \gg \sigma_{inc}^{anion}$). The measured spectra can be decomposed into two Lorentzian lines, indicative of two distinct dynamic processes. The slower of these two processes is diffusive in nature, whereas the faster one can be attributed to localized motions. The temperature dependence of the diffusion coefficient of the slow process follows an Arrhenius law, with an activation energy of E_A = 14.8 ± 0.3 kJ/mol. Furthermore, we present here results from experiments with polarized neutrons. These experiments clearly show that the slower of the two observed processes is coherent, while the faster one is incoherent in nature.

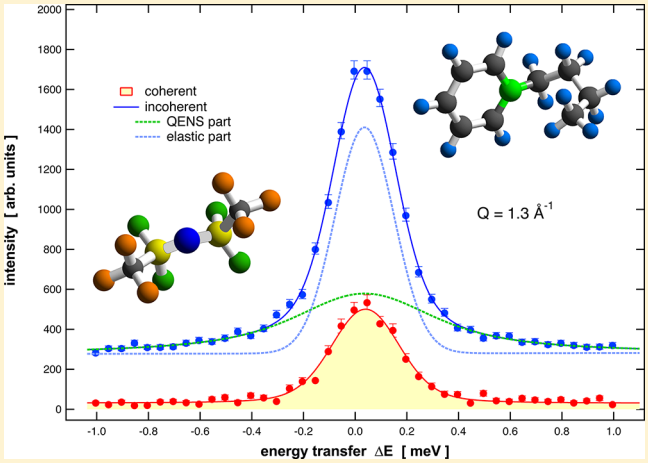

INTRODUCTION

The materials class of ionic liquids (ILs) has attracted considerable research interest in the past few years, and substantial progress has been achieved with respect to the knowledge of thermodynamic and transport characteristics of these compounds. Concerning the structures of ILs, there is a huge number of research papers published on experimental investigations as well as theoretical investigations.[1−14] However, the understanding of dynamic properties in ILs is still limited and many open questions remain to be answered. From recent simulations on ILs and also from experimental studies it became clear that the dynamics in these liquids is decidedly heterogeneous.[5,8,12,13,15−22] Giraud[23] et al. studied the influence of cation and anion substitution on the ultrafast solvent dynamics of ILs by means of optical Kerr effect (OKE) spectroscopy. The authors found three excitations in the wavenumber range between 30 and 100 cm^{-1}; these excitations have been attributed to out-of-plane librations of the imidazolium ring of the cation. Later on, Xiao[24−26] et al. studied the anion effect in ILs with 1,3-pentylmethylimidazolium cations, using the OKE method. The authors focused on the temperature dependence of the OKE spectra; the observed temperature dependence is attributed to the existence of inhomogeneities in the densities in these ILs, and the densities are assumed to result from nanostructurally organized domains in the ILs, i.e., polar and nonpolar regions. The existence of microphase segregation into polar and nonpolar domains in ILs was later on extensively studied by means of molecular dynamics (MD) simulation techniques. Voth and Wang[27] studied the influence of the length of the alkyl side chain in imidazolium based ILs on the aggregation of tail groups in these fluids. Upon increasing the number of carbon atoms, denoted by the capital letter "C", in the side chain, no aggregation of tail groups occurs up to $C = 3$, whereas for $4 \leq C \leq 8$ an aggregation was observed. The case $C = 3$ can be considered as a transition point dividing the liquids into those with and without tail aggregation on a microscopic scale. Lopes[28] and co-workers investigated the solvation of polar, nonpolar, and association solutes in imidazolium based ILs; they found a site selective interaction between the solvent and the solute. The interaction of polar and nonpolar species was found to take place mainly with the cation.

By using MD simulation techniques, Hu and Margulis[29] investigated the dynamics in the IL [1-butyl-3-methylimidazolium]$^+PF_6^-$. Considering the mean square displacement (MSD), three distinct regions have been found: a ballistic region at short times, an intermediate *cage* region, and a diffusive region at long times. Especially the behavior at intermediate times is of great interest since this plateaulike region is characteristic for supercooled liquids. By analyzing the

Received: July 16, 2012
Revised: September 11, 2012
Published: September 28, 2012

 © 2012 American Chemical Society dx.doi.org/10.1021/jp3070344 | *J. Phys. Chem. B* 2012, 116, 13265−13271

van Hove correlation function, it was found that most particles move slower than expected from normal or Fickian diffusion; at the same time there exist subsets of particles moving much faster. Finally, it is stated in this paper that the subgroups (both slow and fast) appear to be correlated in space. For supercooled liquids it is well-known that the dynamic processes are slowed down prior to the transition to a glassy state; close to this transition, the dynamics in one region can be orders of magnitude faster than the dynamics in a neighboring region only a few nanometers away; this is called spatially heterogeneous dynamics. This is in marked contrast to simple or ordinary liquids which are homogeneous. The first paper on quasielastic neutron scattering (QENS) investigations on 1-*n*-butyl-3-methylimidazolium hexaphosphate was published by Triolo and co-workers.[30] In the temperature range between 250 and 320 K two different relaxation processes have been observed. The faster of the two motions shows neither a *Q*- nor a *T*-dependence; this fast β-process was attributed to the motion of the molecules inside a cage. The slow α-process, on the other hand, shows a non-Debye and non-Arrhenius behavior. A recently published paper[31] deals with the investigation of the protic ionic liquid (PIL) *N*,*N*,*N*′,*N*′-tetramethylguanidinium bis(perfluoroethylsulfonyl)imide by means of QENS. Above the melting temperature, i.e., in the liquid state, two processes have been observed. The first, slow, process results from a true, unrestricted translational diffusion, whereas the second one, a fast motion, was described as spatially restricted translation diffusion. Habasaki and Ngai[19] also used MD techniques to study the system $[EMIM]^+[NO_3]^-$. They also found signatures of heterogeneous dynamics in this IL and a strong coupling of the motion of both the anion and the cation. Finally, Del Pópolo and Voth[32] discussed the heterogeneous dynamic behavior and argued that long-living cages must exist, which are formed by neighboring ions; furthermore, they observed a fast rattling of the ions inside the cage. Despite all these efforts, a clear microscopic picture is still missing and thus highly demanded, since the dynamic properties of ILs are assumed to control their macroscopic properties in many ways that are important for possible applications.

EXPERIMENTAL DETAILS

IL Synthesis. We used a two-step process to synthesize protonated as well as completely or partially deuterated IL 1-*N*-butylpyridinium bis((trifluoromethyl)sulfonyl)imide (BuPy-Tf_2N; see Figure 1).

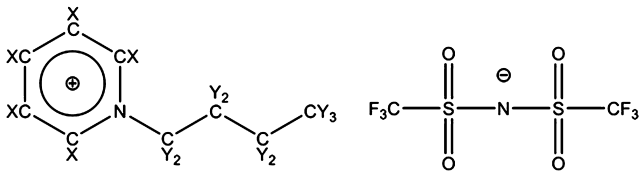

Figure 1. Cation (left) and anion structures of BuPy-Tf_2N. X and Y denote H or D in the case of completely or partially deuterated cation.

In a first step we prepared 1-*N*-butylpyridinium chloride; to do so, pyridine was refluxed in a standard reflux apparatus, fitted with a drying tube, which contained P_2O_5 as drying medium. An equimolar quantity of 1-butyl chloride was slowly added and the reaction mixture was refluxed in a dark environment for 4 days. After cooling to room temperature, the resulting product was crystallized with ethyl acetate (EtOAc) and filtered under vacuum condition; afterward it was washed with EtOAc and quickly transferred into a bottle. The excess of solvent was removed under vacuum at 50 °C for 24 h. The yield of this synthesis step was 87%. In a second step 1-*N*-butylpyridinium chloride was dissolved in distilled water, and an equimolar amount of lithium bis((trifluoromethyl)-sulfonyl)imide was added. The aqueous phase with dissolved LiCl was removed; the remaining ionic liquid was washed five times with distilled water and dried 3 days in a vacuum at 60 °C, resulting in a colorless viscous liquid with a yield of 97%. The water content (<150 ppm) was determined by means of Karl Fischer titration. Furthermore, we used NMR techniques to check the purity and quality of the partial deuteration.

A completely protonated sample of BuPy-Tf_2N has a total scattering cross section about 1275 barns (b); the coherent scattering cross section is about 12% of this value (see Table 1).

Table 1. Summarized Scattering Cross Sections for the Five Different Species Listed in the Text[a]

system	σ_{scatt} [b]	σ_{abs} [b]	σ_{inc} [b]	σ_{coh} [b]
1	1209.75	21.07	1124.15	85.60
2	168.43	6.20	29.21	139.22
3	65.70	9.67	0.52	65.18
4	1275.45	30.74	1124.67	150.78
5	234.13	15.87	29.73	204.40

[a] σ_{abs} is given for neutrons with 5.75 Å incident wavelength.[33] (1 b = 10^{-28} m^2).

From Table 1 we see that the incoherent scattering cross section for the anion amounts only to 0.52 b, whereas the cation exhibits σ_{inc} = 1124.15 b; comparing these two values allows us to conclude that the incoherent scattering cross section of the fluid is given by the one of the cation; i.e., σ_{inc} of the anion can be neglected.

For that reason QENS allows for a detailed investigation of the single-particle dynamics of the cations. The influence of the 12% coherent scattering contribution, due to the C, N, O, and S nuclei, will be discussed later. Table 1 summarizes the scattering cross sections for the following involved species:

1. $C_4H_9-C_5H_5N$, protonated BuPy cation
2. $C_4D_9-C_5D_5N$, completely deuterated BuPy cation
3. $N(SO_2CF_3)_2$, Tf_2N anion
4. IL $[C_4H_9-C_5H_5N]^+[N(SO_2CF_3)_2]^-$
5. IL $[C_4D_9-C_5D_5N]^+[N(SO_2CF_3)_2]^-$

Quasielastic Neutron Scattering (QENS). The method of quasielastic neutron scattering[34] (QENS) is suited to study stochastic, i.e., nonperiodic, dynamic processes in condensed matter. In principle, the method allows for an investigation of true (long-range) diffusion, localized processes (reorientations), and jump diffusive motions. The aim of QENS experiments is to extract diffusion coefficients, jump lengths and reorientation times. Incoherent QENS is very sensitive to samples containing hydrogen due to the large incoherent neutron scattering cross section of the ^1H nucleus. The QENS experiments have been performed on the cold neutron time-of-flight spectrometer (tof) FOCUS[35] at the Swiss spallation source SINQ. For these experiments we used neutrons with an incident wavelength of λ_i = 5.75 Å. The energy resolution at this wavelength is (half-width at half-maximum, hwhm) $\Delta E \approx 22$ μeV. In this study we focus on temperatures at which the IL is in the liquid state. We

dx.doi.org/10.1021/jp3070344 | J. Phys. Chem. B 2012, 116, 13265−13271

used double-walled cylindrical sample containers made of Al. The distance between the inner and outer cylinder was 0.2 mm; this thickness for the sample guarantees neutron transmission of >90% and thus suppresses multiple scattering. The measured intensities of a vanadium standard (of the same shape as the sample) have been used to calibrate the detectors; furthermore, these data have been used to determine the resolution of the spectrometer. We employed measurement times of about 6 h for each temperature. The DAVE[36] software package was used for data reduction (including corrections for self-shielding effects) and analysis. Data measured at constant scattering angles 2θ as function of the time of flight were transformed into $Q-E$ space. These data were binned into 14 groups of constant Q values; the energy range was set to ±1 meV. An example of a $S(Q,E)$ spectrum at $Q = 1.1$ Å^{-1} is shown in Figure 2, together with the residuals as obtained by fitting the experimental data with an appropriate model (see the section Data Analysis for further details).

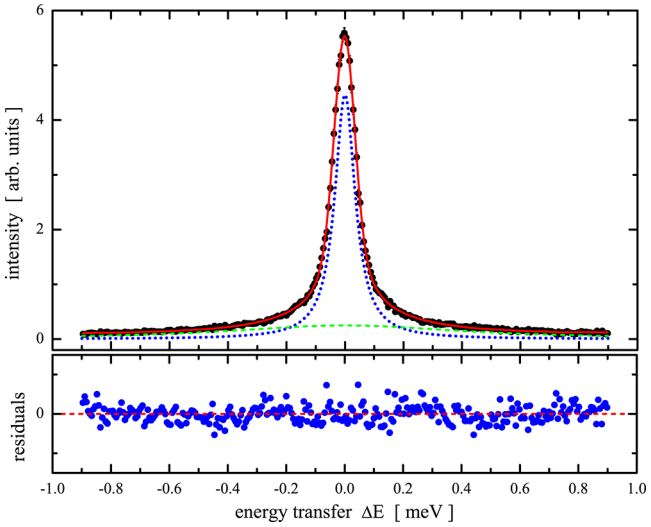

Figure 2. Upper panel: QENS spectrum of a completely protonated BuPy-Tf$_2$N sample, measured at 340 K and $Q = 1.1$ Å^{-1} (symbols) together with the fit function (red solid line), described in the text. The dotted and dashed functions shown in the upper panel represent Lorentzian functions, of which the solid line is composed. In the lower panel the residuals between the fit function and the measured intensities are shown.

Data Analysis. Model independent fits show that the measured quasielastic spectra can be very well described as a superposition of two Lorentzian curves and a linear background (see Figure 2); i.e., no elastic contribution is present in all measured spectra. Inspired by QENS results obtained on other complex systems, such as proteins[37,38] or medium-chain alkanes,[39] we consider for our sample a dynamic structure factor, which includes both local processes (for example, librations of the alkyl chain and methyl end group rotations) and a global process[40] which involves the cation as a whole. Based on these assumptions, the dynamic structure factor $S(Q,E)$ reads

$$S(Q, E) = S_{\text{local}}(Q, E) \otimes S_{\text{global}}(Q, E) \quad (1)$$

with the following expressions for the local and global dynamic structure factors, respectively:

$$S_{\text{local}}(Q, E) = A(Q)\,\delta(E) + [1 - A(Q)]\frac{1}{\pi}\frac{\Gamma_1(Q)}{\Gamma_1^2(Q) + E^2} \quad (2)$$

$$S_{\text{global}}(Q, E) = \frac{1}{\pi}\frac{\Gamma_2(Q)}{\Gamma_2^2(Q) + E^2} \quad (3)$$

$A(Q)$ in eq 2 represents the elastic incoherent structure factor (EISF) of the localized motion and describes the geometry of the spatial confinement in which the localized processes take place; the two line widths Γ_1 and Γ_2 describe the broadening in energy space caused by the local and global dynamic processes, respectively. The following form of the dynamic structure factor was used to fit the data:

$$S_I(Q, E) = I_0(Q)\cdot[S(Q, E) \otimes R(Q, E)] + a + bE \quad (4)$$

The factor $I_0(Q)$ contains an intensity factor and the Debye–Waller factor. With $R(Q,E)$ we denote the resolution function (experimentally determined by measuring a standard Vandium sample), and the term $a + bE$ represents a linear background. The convolution (denoted by the symbol ⊗ in eq 1) is performed numerically using the PAN package as included in the DAVE software. In Figure 2 we show a spectrum taken at 340 K and $Q = 1.1$ Å^{-1}. The solid line in the upper panel of Figure 2 represents a fit according to eqs 2–4 (the dotted and dashed curves represent the two components of the model that is used to describe the data). A closer inspection of the line widths $\Gamma_2(Q)$ shows that these can be very well described by a jump-diffusion model proposed by Singwi and Sjölander.[41] The line widths in this model are given by

$$\Gamma_2(Q) = \frac{\hbar D_s Q^2}{1 + D_s Q^2 \tau_0} \quad (5)$$

In eq 5, D_s is the self-diffusion coefficient for the observed process and with τ_0 we denote the residence time, i.e., the time the particle spends at a position before performing the next jump event and thus reaching a new position.

RESULTS AND DISCUSSION

In Figure 3 we show the line width (hwhm) Γ_2 as a function of Q^2, for different temperatures. The data were fitted with eqs 2–4, with the fits represented by dashed lines; from the fitting procedure we extracted the diffusion coefficient D_s and the residence time τ_0, respectively, using eq 5.

Both the residence times and the diffusion coefficients are plotted as a function of the inverse temperature in Figure 4.

The temperature dependence of the self-diffusion coefficient, D_s (see Figure 4), can be modeled by the following Arrhenius equation:

$$D_s(T) = D_0 \exp[-E_A/RT] \quad (6)$$

R denotes the gas constant and E_A is the activation energy for the corresponding process; the fit result is $E_A = 14.8 \pm 0.3$ kJ/mol. The solid line in Figure 4 (lower panel) represents the result obtained by Tokuda et al.[42] using NMR methods. The difference between our result and the latter is most likely caused by the different time scales in which the two experimental methods operate. With QENS (operating on an angstrom length and picosecond time scale) we get the short-time diffusion coefficient, whereas with NMR (usually working in micrometer length and microsecond time scale) methods the long-time diffusion coefficient is probed.[43]

dx.doi.org/10.1021/jp3070344 | J. Phys. Chem. B 2012, 116, 13265–13271

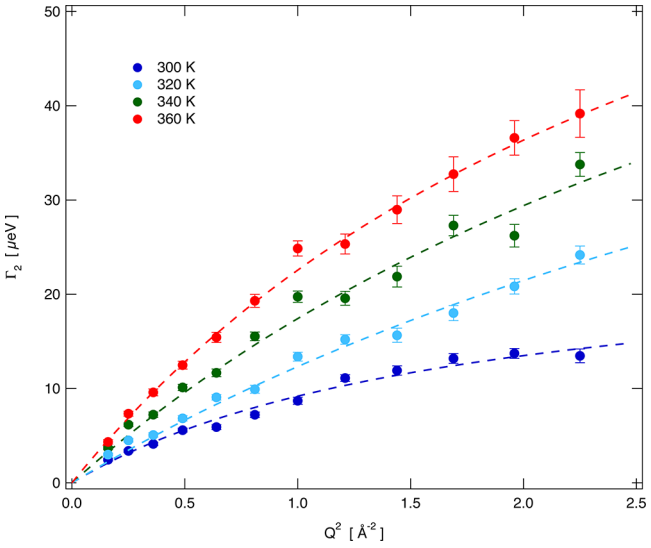

Figure 3. Line width Γ_2 (hwhm) as a function of Q^2 for four different temperatures. The dashed lines are fits according to eq 5.

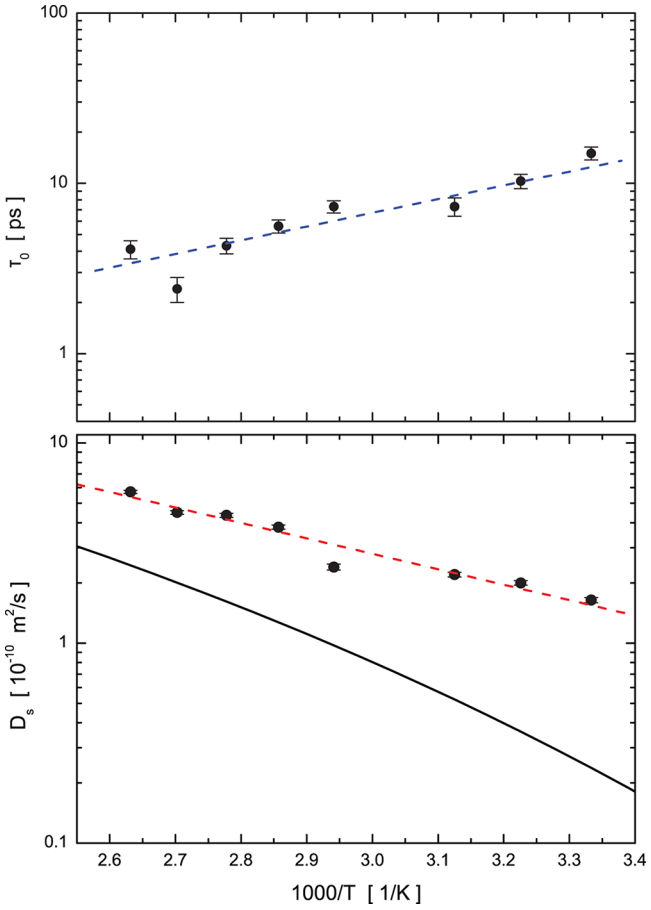

Figure 4. Upper panel: residence time τ_0 as a function of the inverse temperature (the dashed line is a guide for the eyes). Lower panel: diffusion coefficient D_s as a function of the inverse temperature; the dashed line represents a fit according to eq 6. The solid line represents the temperature dependence of the diffusion coefficient as observed by NMR techniques.[42]

To change the scattering situation from being dominated by incoherent scattering to a situation in which the coherent scattering dominates, we investigated also a completely deuterated IL sample. In Figure 5 we compare the line width of the slow process as observed by fitting the spectra with the model for the dynamic structure factor $S(Q,E)$ presented in the section Data Analysis.

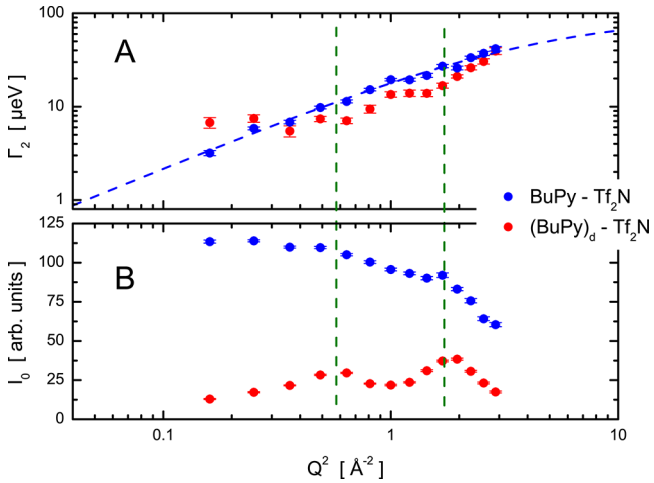

Figure 5. Comparison of fit results for the line width Γ_2 of the slow process obtained from a completely deuterated sample and a completely protonated sample at T = 340 K. The slow process in the deuterated sample, as characterized by the line width Γ_2, shows a clear slowing down at those Q values which correspond to the location of maxima in $S(Q)$. The dashed line is a fit according to eq 6.

Comparing panels A and B in Figure 5, we see that the modulation of Γ_2 and the maxima observed for I_0 correlate with respect to their Q positions. The modulation of Γ_2 for the completely deuterated sample is more pronounced than that for the completely protonated sample; the reason for this is due to the fact that for the latter sample the incoherent scattering dominates while for the completely deuterated sample it is the coherent scattering which has the strongest influence. To check whether the static structure factor $S(Q)$ influences $S(Q,E)$, we used a completely deuterated IL to study the structure of the liquid phase. The measurement was performed on the thermal diffractometer HRPT[44] at the Swiss spallation source SINQ. In Figure 6 we plot the detected intensity as function of the modulus of the scattering wave vector.

From Figure 6 we see that two structural maxima can be observed in the Q range that is covered in our QENS experiments ($Q < 2.0$ Å^{-1}): a first peak at $Q_1 \approx 0.8$ Å^{-1} ($R_1 = 2\pi/Q_1 \approx 7.8$ Å) and a second peak at $Q_2 \approx 1.4$ Å^{-1} ($R_1 \approx 4.5$ Å). These peaks in $S(Q)$ are known in the literature as prepeaks or *first sharp diffraction peaks* (FSDP). For further discussions of these peaks we refer to refs 45−47 and references therein. The two maxima occur at similar positions at which the modulations of the line width Γ_2 and the corresponding intensity I_0 can be observed; see Figure 5. This implies that the observed modulations in Γ_2 and I_0 are due to $S(Q)$ and thus reflect the influence of coherent scattering. The observed effect was first predicted theoretically by de Gennes.[48] This effect has been observed experimentally measuring the transport properties of H_2 and D_2 in NaX zeolites[49] and in investigations on the stochastic dynamics in molten potassium using polarized QENS.[50]

The most interesting finding, in this context, is the fact that the fast dynamic process remains unchanged by the static structure factor, as can be seen by inspection of Figure 7,

dx.doi.org/10.1021/jp3070344 | J. Phys. Chem. B 2012, 116, 13265−13271

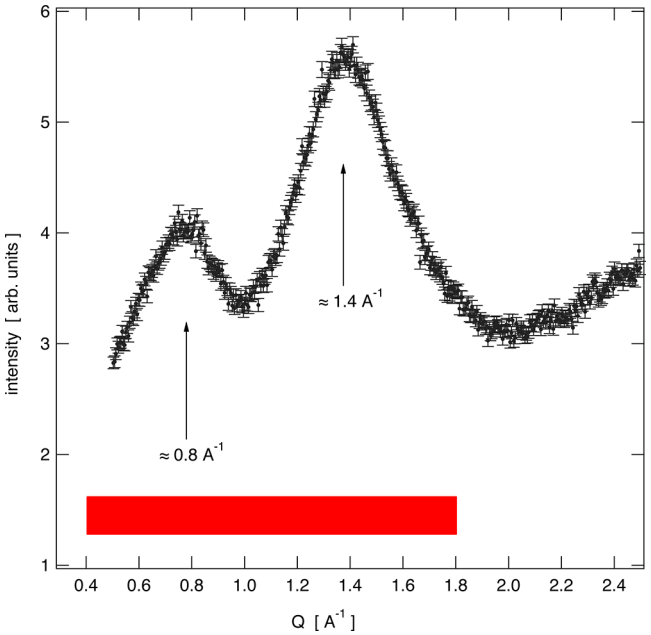

Figure 6. Intensity as function of Q as measured on a completely deuterated sample, BuPy-Tf_2N. This experiment was performed on the thermal neutron diffractometer HRPT at SINQ, using neutrons with λ_i =1.5 Å. The rectangle marks the Q range covered in the QENS experiments.

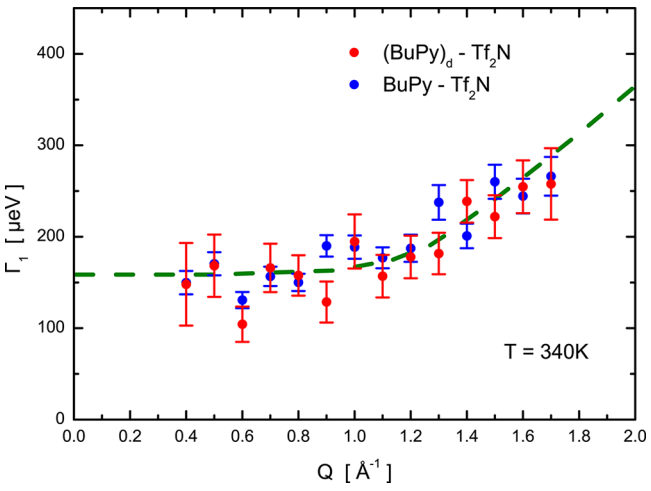

Figure 7. Comparison of fit results from a completely deuterated sample and a completely protonated sample.The dashed line is a guide for the eyes.

showing the line widths $\Gamma_1(Q)$ that characterize the fast dynamic process. For both the completely protonated and the completely deuterated ILs, we observe the same Q dependence (within the experimental errors) of these line widths. This demonstrates that the processes responsible for the observed broadening are not affected by $S(Q)$ and are thus incoherent in nature.

Furthermore, we see a plateaulike behavior in $\Gamma_1(Q)$, which is indicative of a dynamic process inside a spatial confinement; the dashed line in Figure 7 serves as a guide for the eyes. The confinement is most likely due to the surrounding ions, forming a cagelike structure and thus a confinement for the cation. Cages or cagelike structures have been observed in many MD simulations; we would like to point out that these confinements are typical for liquids in the vicinity of the glass transition and are normally not observed far from the glass transition temperature.

So far we used deuteration to alter the ratio between coherent and incoherent scattering contributions. However, it is not possible to bring either the coherent or the incoherent scattering contribution to zero, and therefore a strict separation of these two contributions cannot be reached! The only experimental way to separate coherent and incoherent scattering contributions is to make use of polarized neutrons.[51] Using the following equations, the separation of coherent and incoherent scattering contributions can be performed numerically:

$$I_{coh} = I_{corr}^{\uparrow\uparrow} - \frac{1}{2} I_{corr}^{\uparrow\downarrow} \tag{7}$$

$$I_{inc} = \frac{3}{2} I_{corr}^{\uparrow\downarrow} \tag{8}$$

with

$$I_{corr}^{\uparrow\uparrow} = I^{\uparrow\uparrow} + \frac{1}{R-1}[I^{\uparrow\uparrow} - I^{\uparrow\downarrow}] \tag{9}$$

$$I_{corr}^{\uparrow\downarrow} = I^{\uparrow\downarrow} - \frac{1}{R-1}[I^{\uparrow\uparrow} - I^{\uparrow\downarrow}] \tag{10}$$

In eqs 9 and 10, R denotes the (finite) flipping ratio for the complete experimental setup (as determined with a SiO_2 (quartz) standard), and $I^{\uparrow\uparrow}$ and $I^{\uparrow\downarrow}$ represent the experimentally determined (so-called) non-spin-flip and spin-flip intensities, respectively.

In Figure 8 we present results obtained with the triple-axis spectrometer TASP[52] at SINQ. This measurement has been performed at Q = 1.3 Å^{-1}, with an experimental resolution of 0.27 meV (full width at half-maximum, fwhm). The incoherent spectrum was fitted by

$$\left[A(Q)\,\delta(E) + [1 - A(Q)]\frac{1}{\pi}\frac{\Gamma_1(Q)}{\Gamma_1^2(Q) + E^2}\right] \otimes R(Q, E) \tag{11}$$

(see eqs 2 and 4), whereas for the coherent spectrum we used the following expression to describe the data:

$$\left[\frac{1}{\pi}\frac{\Gamma_2(Q)}{\Gamma_2^2(Q) + E^2}\right] \otimes R(Q, E) \tag{12}$$

(see eqs 3 and 4). This result (obtained so far at one Q value only) strongly corroborates our assumption that the slow process is coherent, while the fast dynamics is a true single particle (i.e., incoherent) process. Figure 8 shows the coherent data together with the best fit according to eq 12; at this point we have to point out that the coherent data show a clear broadening with an fwhm of 76 ± 18 μeV. The incoherent data are plotted in Figure 8 together with the total fit function (solid line) and the two fit components according to eq 11.

CONCLUSIONS

We used quasielastic neutron scattering to investigate the dynamic properties of the cation of the IL 1-*N*-butylpyridinium bis((trifluoromethyl)sulfonyl)imide. Quasielastic neutron scattering experiments, performed in the liquid state of the corresponding IL, indicate two different dynamic processes, which take place on very different time scales. The first (slow)

dx.doi.org/10.1021/jp3070344 | J. Phys. Chem. B 2012, 116, 13265−13271

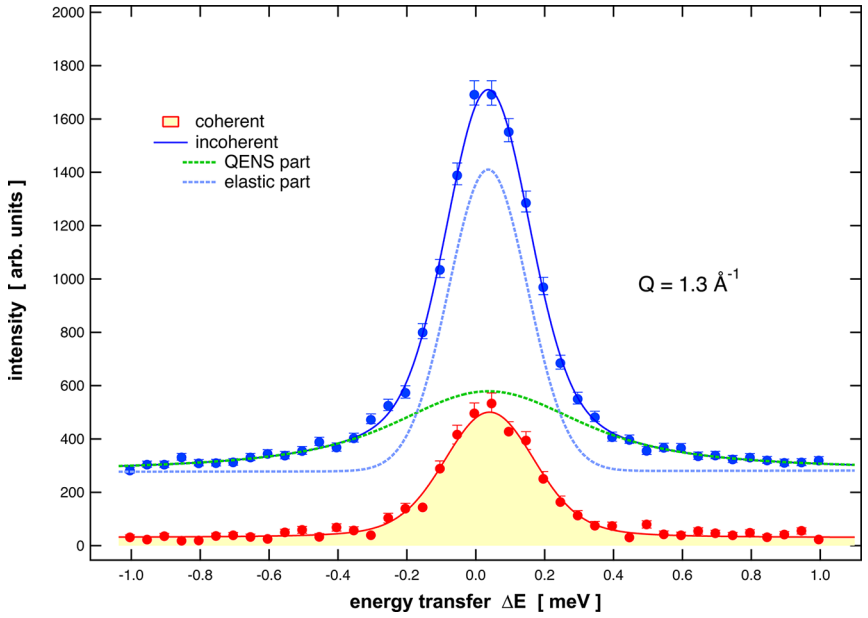

Figure 8. Incoherent (upper spectrum) and coherent (lower spectrum) parts of the dynamic structure factor $S(Q,E)$ as measured on the spectrometer TASP[52] at room temperature using polarized neutrons. The upper, incoherent spectrum can be decomposed into an elastic and a quasielastic part, and the lower, coherent spectrum is purely quasielastic; i.e., no elastic contribution was observed. The incoherent spectrum is shifted upward for clarity.

process is diffusive in nature; the line width, which corresponds to this process, can be very well described in terms of a jump diffusion process. By investigating a completely deuterated sample and comparing the line width of the slow process for both samples, we can conclude that this process contains (in addition to incoherent scattering contribution) also coherent scattering components, thus being (at least partially) of collective nature. Using polarized neutrons (to our knowledge for the first time on an IL), we can confirm this statement. In future experiments we will extend the accessible Q range further to investigate these findings in more detail.

The second (fast) process we observe is not affected by the structure, i.e., by the static structure factor $S(Q)$. This experimental finding allows us to conclude that the fast process is a true single particle motion, reflecting the single particle dynamic behavior on a short time scale. The fact that the line width of this process shows up with a plateau can be interpreted as resulting from processes that take place inside (spherical) confinements. The very general model we use to describe the QENS data describes in a reasonable way the dynamic processes in the IL as observed with the instrumental resolution used. The dynamic processes in ILs are complex due to the complexity of the ions which constitute the corresponding IL. In fact, any stochastic motion of the cation or of parts of the cation, e.g., of the alkyl chain or the pyridinium ring, contribute to the quasielastic signal. The method used here to follow the dynamic processes measures a superposition of signals resulting from all possible processes. We will extend our investigations on ILs with increasing alkyl chain length (the basic cation and anion will remain unchanged) to study the influence of this length on the dynamic behavior that is observed with quasielastic neutron scattering as well as with fixed energy window scans. Finally, we will compare our results to results obtained with MD methods (classical MD as well as ab initio MD simulations); due to the complexity of the ions, the dynamic scenario is very complex as well and thus a combination of experiment and simulation is highly demanded.

AUTHOR INFORMATION

Corresponding Author

*E-mail: jan.embs@psi.ch.

Notes

The authors declare no competing financial interest.

ACKNOWLEDGMENTS

Financial support by the Deutsche Forschungsgemeinschaft (DFG) within the Scientific Priority Program SPP 1191 Ionic Liquids is gratefully acknowledged. This work is based on experiments performed at the Swiss spallation source SINQ, Paul Scherrer Institut, Villigen, Switzerland. The FOCUS spectrometer at the Swiss spallation neutron source SINQ, Paul Scherrer Institute, Villigen, Switzerland, has financially been supported by the BMBF in the framework of Forschung mit Großgeräten. We would like to thank B. Kirchner (University of Leipzig) and R. Buchner (University of Regensburg) for stimulating and fruitful discussions. Finally, we thank D. Cheptiakov for performing the diffraction experiments on the completely deuterated IL and B. Roessli for help and fruitful discussions during the TASP experiments.

REFERENCES

(1) Zahn, S.; Thar, J.; Kirchner, B. *J. Chem. Phys.* **2010**, *132*, 124506.
(2) Bedrov, D.; Borodin, O.; Li, Z.; Smith, G. D. *J. Phys. Chem. B* **2010**, *114*, 4984−4997.
(3) Wang, Y. *J. Phys. Chem. B* **2009**, *113*, 11058−11060.
(4) Gontrani, L.; Russina, O.; Celso, F. L.; Caminiti, R.; Annat, G.; Triolo, A. *J. Phys. Chem. B* **2009**, *113*, 9235−9240.
(5) Spohr, H. V.; Patey, G. N. *J. Chem. Phys.* **2009**, *130*, 104506.
(6) Hardacre, C.; Holbrey, J. D.; Mullan, C. L.; Nieuwenhuyzen, M.; Youngs, T. G.; Bowron, D. T. *J. Phys. Chem. B* **2008**, *112*, 8049−8056.
(7) Fujii, K.; Soejima, Y.; Kyoshoin, Y.; Fukuda, S.; Kanzaki, R.; Umebayashi, Y.; Yamaguchi, T.; Ishiguro, S.; Takamuko, T. *J. Phys. Chem. B* **2008**, *112*, 4329−4336.
(8) Koddermann, T.; Paschek, D.; Ludwig, R. *ChemPhysChem* **2007**, *8*, 2464−2470.

(9) Ghatee, M. H.; Ansari, Y. *J. Chem. Phys.* **2007**, *126*, 154502.
(10) Sloutskin, E.; Lyndell-Bell, R. M.; Balasubramanian, S.; Deutsch, M. *J. Chem. Phys.* **2006**, *125*, 174715.
(11) Pinilla, C.; Popolo, M.; Lyndell-Bell, R. M.; Kohanoff, J. *J. Phys. Chem. B* **2005**, *109*, 17922−17927.
(12) Borodin, O.; Smith, G. D. *J. Phys. Chem. B* **2006**, *110*, 11481−11490.
(13) Costa, L. T.; Ribeiro, M. C. *J. Chem. Phys.* **2006**, *124*, 184902.
(14) Yan, T.; Li, S.; Jiang, W.; Gao, X.; Xiang, B.; Voth, G. A. *J. Phys. Chem. B* **2006**, *110*, 1800−1806.
(15) Jeong, D.; Choi, M. Y.; Kim, H. J.; Jung, Y. *Phys. Chem. Chem. Phys.* **2010**, *12*, 2001−2010.
(16) Kowsari, M. H.; Alavi, S.; Ashrafizaadeh, M.; Najafi, B. *J. Chem. Phys.* **2010**, *132*, 044507.
(17) Kowsari, M. H.; Alavi, S.; Ashrafizaadeh, M.; Najafi, B. *J. Chem. Phys.* **2008**, *129*, 224508.
(18) Spickermann, C.; Thar, J.; Lehmann, S. B.; Zahn, S.; Hunger, J.; Buchner, R.; Hunt, P. A.; Welton, T.; Kirchner, B. *J. Chem. Phys.* **2008**, *129*, 104505.
(19) Habasaki, J.; Ngai, K. L. *J. Chem. Phys.* **2008**, *129*, 194501.
(20) Siqueira, L. J.; Ribeiro, M. C. *J. Phys. Chem. B* **2007**, *111*, 11776−11785.
(21) Bhargava, B. L.; Balasubramanian, S. *J. Phys. Chem. B* **2007**, *111*, 4477−4487.
(22) Urahata, S. M.; Ribeiro, M. C. *J. Chem. Phys.* **2006**, *124*, 74513.
(23) Giraud, G.; Gordon, C. M.; Dunkin, I. R.; Wynne, K. *J. Chem. Phys.* **2003**, *119*, 464−477.
(24) Xiao, D.; Hines, L. G.; Li, S.; Bartsch, R. A.; Quitevis, E. L.; Russina, O.; Triolo, A. *J. Phys. Chem. B* **2009**, *113*, 6426−6433.
(25) Xiao, D.; Rajian, J. R.; Cady, A.; Li, S.; Bartsch, R. A.; Quitevis, E. L. *J. Phys. Chem. B* **2007**, *111*, 4669−4677.
(26) Xiao, D.; Rajian, J. R.; Hines, L. G.; Li, S. F.; Bartsch, R. A.; Quitevis, E. L. *J. Phys. Chem. B* **2008**, *112*, 13316−13325.
(27) Wang, Y.; Voth, G. A. *J. Am. Chem. Soc.* **2005**, *127*, 12192−12193.
(28) Lopes, J. N. C.; Gomes, M. F. C.; Padua, A. A. H. *J. Phys. Chem. B* **2006**, *110*, 16816−16818.
(29) Hu, Z. H.; Margulis, C. J. *Proc. Natl. Acad. Sci. U.S.A.* **2006**, *103*, 831−836.
(30) Triolo, A.; Russina, O.; Arrighi, V.; Juranyi, F.; Janssen, S.; Gordon, C. M. *J. Chem. Phys.* **2003**, *119*, 8549−8557.
(31) Mammontov, E.; Luo, H.; Dai, S. *J. Phys. Chem. B* **2009**, *113*, 159−169.
(32) Del Pópolo, M. G.; Voth, G. A. *J. Phys. Chem. B* **2004**, *108*, 1744−1752.
(33) http://www.ncnr.nist.gov/resources/n-lengths.
(34) Hempelmann, R. *Quasielastic Neutron Scattering and Solid State Diffusion*; Clarendon Press, Oxford University Press: New York, 2000.
(35) Janssen, S.; Mesot, J.; Holitzner, L.; Furrer, A.; Hempelmann, R. *Physica B* **1997**, *234*, 1174−1176.
(36) Azuah, R. T.; Kneller, L. R.; Qiu, Y. M.; Tregenna-Piggott, P.; Brown, C. M.; Copley, J. R. D.; Dimeo, R. M. *J. Res. Natl. Inst. Stand.* **2009**, *114*, 341−358.
(37) Stadler, A. M.; van Eijck, L.; Demmel, F.; Artmann, G. *J. R. Soc., Interface* **2011**, *8*, 590−600.
(38) Smuda, C.; Busche, S.; Gemmecker, G.; Unruh, T. *J. Chem. Phys.* **2008**, *128*, 194502.
(39) Smuda, Ch.; Busch, S.; Gemmecker, G.; Unruh, T. *J. Chem. Phys.* **2008**, *129*, 014513.
(40) Sharma, V. K.; Mitra, S.; Verma, G.; Hassan, P. A.; Sakai, V.; Mukhopadyay, R. *J. Phys. Chem. B* **2010**, *114*, 17049−17056.
(41) Singwi, K. S.; Sjölander, A. *Phys. Rev.* **1960**, *119*, 863−871.
(42) Tokuda, H.; Ishii, K.; Susan, M. A. B. H.; Tsuzuki, S.; Hayamizu, K.; Watanabe, M. *J. Phys. Chem. B* **2006**, *110*, 2833−2839.
(43) Wuttke, J.; Chang, I.; Randl, O. G.; Fujara, F.; Petry, W. *Phys. Rev. E* **1993**, *54*, 5364−5369.
(44) Fischer, P.; Frey, G.; Koch, M.; Könnecke, M.; Pomjakushin, V.; Schefer, J.; Thut, R.; Schlumpf, N.; Bürge, R.; Greuter, U.; Bondt, S.; Berruyer, E. *Physica B* **2000**, 276−278.
(45) Castner, E. W., Jr.; Margulis, C. J.; Maroncelli, M.; Wishart, J. F. *Annu. Rev. Phys. Chem.* **2011**, *62*, 85−105.
(46) Song, X.; Hamano, H.; Minofar, B.; Kanzaki, R.; Fujii, K.; Kameda, Y.; Kohara, S.; Watanabe, M.; Ishiguro, S.; Umebayashi, Y. *J. Phys. Chem. B* **2012**, *116*, 2801−2813.
(47) Annapureddy, H. V. R.; Kashyap, H. K.; Biase, P.; Margulis, C. J. *J. Phys. Chem. B* **2010**, *114*, 16838−16846.
(48) de Gennes, P. *Physica (Utrecht)* **1959**, *25*, 825−839.
(49) Jobic, H.; Kärger, J.; Bée, M. *Phys. Rev. Lett.* **1999**, *82*, 4260−4263.
(50) Ruiz-Martín, M. D.; Jiménez-Ruiz, M.; Stunault, A.; Bermejo, F. J.; Fernández-Perea, R.; Cabrillo, C. *Phys. Rev. B* **2007**, *76*, 174201.
(51) Schärpf, O.; Capellmann, H. *Phys. Status Solidi A* **1993**, *135*, 359−379.
(52) Semadeni, F.; Roessli, B.; Böni, P. *Physica B* **2001**, *297*, 152−154.